IOP Publishing Journal of Physics D: Applied Physics
J. Phys. D: Appl. Phys. **48** (2015) 385501 (7pp) doi:10.1088/0022-3727/48/38/385501

Heat generation of mechanically abused lithium-ion batteries modified by carbon black micro-particulates

Anh V Le[1], Meng Wang[1], Yang Shi[2], Daniel J Noelle[2] and Yu Qiao[1]

[1] Department of Structural Engineering, University of California—San Diego, La Jolla, CA 92093-0085, USA
[2] Program of Materials Science and Engineering, University of California—San Diego, La Jolla, CA 92093, USA

E-mail: yqiao@ucsd.edu

Received 27 March 2015, revised 25 June 2015
Accepted for publication 6 July 2015
Published 25 August 2015

Abstract

In the current study, we experimentally investigated the effects of carbon black micro-particulates (CBMP) on the temperature increase of lithium-ion battery coin cells subjected to nail penetration and blunt impact. The major difference between CBMP and regular carbon black additives is in particle size. The testing data showed that addition of 1 wt% of CBMP in the cathode and anode does not influence the cycle life, while can reduce the heat generation rate by nearly 50%, after the peak temperature is reached. Thermal treatment of the modified cells at 100 °C would further reduce the heat generate rate. The initial temperature increase rate, the maximum temperature, as well as the total energy dissipation are not affected. These findings shed light on thermal runaway mitigation of high-energy batteries.

Keywords: lithium-ion battery, micro-particulate, thermal runaway, impact, nail penetration

(Some figures may appear in colour only in the online journal)

1. Introduction

Developing robust, high-performance lithium-ion batteries is critical to a large number of engineering applications, such as smart grids, electric vehicles, high-energy power sources, etc [1, 2]. Many other energy storage techniques, e.g. zinc air batteries [3], flow batteries [4], lithium-sulfur batteries [5], fuel cells [6], and graphene-based electrochemical microsupercapacitors [7], are still in the early laboratory research stage. The main components of a Li-ion battery cell include a cathode on aluminum (Al) charge collector and an anode on copper (Cu) charge collector, with a thin porous membrane separator sandwiched in between, and 15–20 wt% electrolyte. Usually, the electrodes are produced through slurry processing, consisting of active materials, polymer binder, and carbon black (CB) [8]. While the most important factor that determines the battery performance is the active materials, there are many other critical engineering parameters, e.g. the type and the content of polymer binder as well as the morphology of CB.

There has not been a generally accepted design protocol for the CB material. The electrical conductivity of a single CB particle is quite high. However, uniformly mixing CB particles with active material and efficiently improving electrode quality are non-trivial. Controlling the CB particle size helps enhance the bulk distribution of the conductive phase [9], and may lead to a lower materials cost and a simpler slurry processing procedure. The CB particle size effects on various battery behaviors, including the temperature increase during thermal runaway, are still poorly understood.

Under normal working condition, the membrane separator keeps the cathode and the anode away from each other. During normal operation, heat generation of a Li-ion battery cell is usually mild, and can be well handled by the battery management system (BMS) and the battery thermal management system (BTMS) [10]. If the battery cell is damaged, e.g. by a blunt impact or nail penetration, the membrane separator is broken apart, leading to the internal shorting. As a large internal current is generated, local temperature can rapidly

 © 2015 IOP Publishing Ltd Printed in the UK

rises to more than 100–110 °C, which further triggers exothermal electrochemical reactions and decomposition of electrolyte. Since the electrolytes of today's Li-ion batteries are based on flammable organic solvents, such as dimethyl carbonate (DMC), ethyl methyl carbonate (EMC), and/or diethyl carbonate (DEC), fire safety becomes a major concern. Several studies have been conducted to mitigate the heat generation in the event of mechanical abuse, including safety vents, shutdown separators, non-flammable electrolyte, etc [11]. In this study, we focus on the CB particles.

If the CB particle size is relatively large, around tens of μm, it may influence the internal shorting. On the one hand, it is easier for large CB micro-particulates (CBMP) to form conductive bridges across the damaged membrane, and therefore, heat generation may be promoted. On the other hand, large CBMP could store more elastic energy as the electrodes are pressurized, which leads to debonding along matrix-filler interfaces [12]; such CBMP become damage homogenizers (DH) [13]. With the widespread interface cracking, the internal impedance of the battery system rises, suppressing the internal shorting current and heat generation. Currently, there is still no experimental result showing which mechanism is dominant.

In the current study, we investigate the effects of adding large CBMP in the electrodes of CR2016 coin cells that are subjected to mechanical abuse. Cycle life testing is carried out on the CBMP modified cells to identify the optimum CBMP content.

2. Experimental

For the positive electrodes, the active material (AM) was chosen as $LiNi_{0.5}Mn_{0.3}Co_{0.2}O_2$ (NMC532) (NCM-04ST from TODA America), with an average particle size of 10–20 μm. The binder was polyvinylidene fluoride (PVDF) with the molecular weight, M_w, of 534 k (Product No. 182702 from Sigma-Aldrich). The conductive additive was carbon black (CB) nanoparticles (CNERGY-C65 from TIMCΛL). The weight ratio among them was 93:4:3. The anodes were made from artificial graphite (AG) powders (EQ-Lib-CMSG from MTI); the weight ratio among the solid components, i.e. AG, PVDF, and CB, was 93:6:1. The CBMP under investigation was Norit-Cabot C-Gran. The nominal mass density was 0.2 g cm^{-3}; the specific surface area was 1400 m^2 g^{-1}; the average particulate size was ~45 μm; the material was hydrophilic.

To process reference cathodes, about 5 g of AM, PVDF, and CB were ground and mixed in a set of agate mortar and pestle for 45 min. To produce modified cathodes, 1–5 wt% CBMP was added prior to the grinding and mixing. The mixture was then transferred to a 10 mL beaker, and 2 mL of NMP (Product No. 328634 from Sigma-Aldrich) was added and thoroughly mixed by a Qsonica Q55 ultrasonic processor for about 30 min. The mixing was interrupted periodically to avoid overheating. The anode slurry was prepared through a similar procedure.

Casting of wet slurries was performed using a doctor blade, and the slurries were dried at 100 °C in vacuum for 24 h. The cathode slurry thickness was either 100 μm (for cycle life testing) or 200 μm (for impact and nail testing); the anode slurry thickness was either 50 μm (for cycle life testing) or 100 μm (for impact and nail testing). After drying, the slurry thicknesses were 40–50 μm and 100–110 μm for thin and thick cathodes, respectively, and 20–30 μm and 60–70 μm for thin and thick anodes, respectively.

The dried slurry was compressed by a hardened steel double roller, and cut into circular disks with the diameter of 14.3 mm. A full battery cell contained a cathode and an anode. The active material mass of a thin cathode was 18–20 mg, or 30–35 mg for a thick cathode. The active material mass in anode was about 50% of that of cathode. Each pair of positive electrode and negative electrode with compatible masses were placed in a standard set of CR2016 coin cell case (Product No. T-2016 from Xiamen Tob), separated by a single 25 μm thick porous PP/PE/PP tri-layer membrane separator (Product No. 2325 from Celgard). The active cell components were secured by a set of stainless steel spacers and springs for impact test, and by a nickel foam for nail penetration test. Finally, sufficient BASF SelectiLyte-LP50 EC/EMC electrolyte was added.

Cathode half-cells were produced through a similar procedure as the full cells, except that in the final cell assembly step the anode was replaced by a lithium disk with the diameter of 15.4 mm and the thickness of 1.1 mm, without any spacer or spring.

The battery cells were at rest for 24 h for full electrolyte diffusion. Cells of thinner electrodes were tested for electrochemical performance for 100 charge-discharge cycles, in an MIT BST8-3 Battery Analyzer. Cells of thicker electrodes were charged-discharged for at least 5 cycles with the voltage range of 3–4.3 V and then charged to 4.6 V using the same battery analyzer. The final voltage was higher than that of cycling test but within the stable range. Immediately after charging, there would be a slight voltage drop from 4.6 V to 4.54–4.56 V, which was observed for both reference and modified cathode half-cells. At rest, stable cell voltage was maintained at 4.54–4.56 V for about 2 h.

Nail penetration tests were carried out on fully charged cells on a solid polyurethane (PU) platform (figure 1). The cell was firmly attached on the platform by 5 layers of insulating tapes and indented upon by a stainless steel nail with the diameter of 1.58 mm. The nail was placed inside a PU foam that insulated the cell from the environment, and driven by a Palmgren bench vise. An Omega TT-K-40-25 type-K gage 40 thermal couple was adhered within 2.5 mm from the center of the cell (figure 1), connected to an Omega OM-EL-USB-TC temperature logger. In some tests, the battery cells were preheated in a VWR 52201–214 horizontal airflow oven at 100 °C for 30 min, and air cooled to room temperature prior to the nail penetration.

Blunt impact tests were performed on fully charged cells on the same solid PU platform. A battery was secured on the platform by insulating tapes and indented upon by a copper spherical indenter with the diameter of 12.7 mm. Initially, the indenter was rested on top of the battery cell, separated by 5 layers of insulating tapes. The system was insulated by a solid

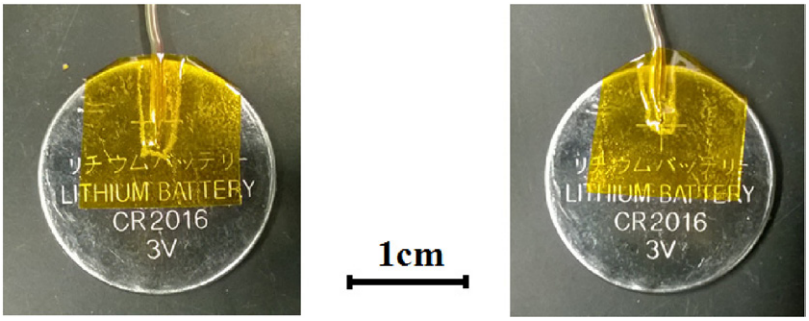

Figure 1. The testing samples. Left: a typical CR2016 coin cell for nail penetration testing, with the thermocouple tip 2.5 mm away from the center. Right: A typical CR2016 cell for blunt impact testing, with the thermocouple tip 5.0 mm away from the center.

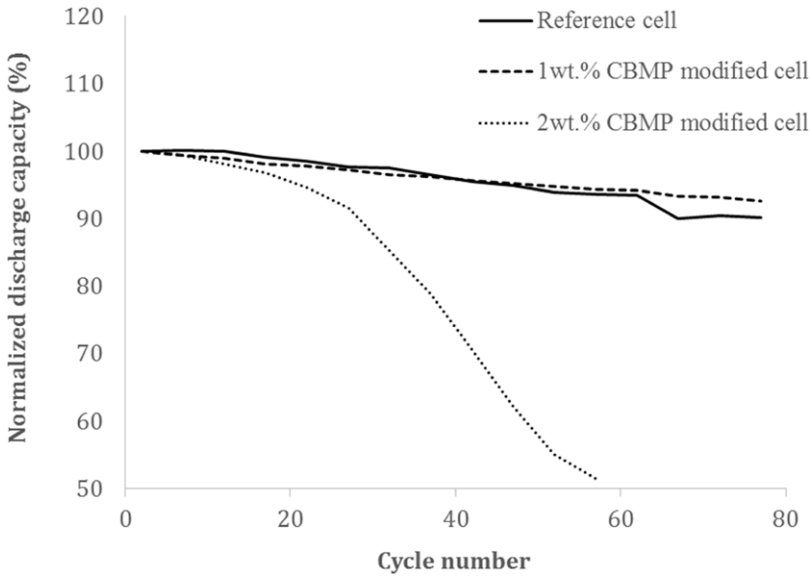

Figure 2. Cycling performance of reference and CBMP-modified cathode half cells.

PU cover, which also acted as the guide for a stainless steel rod with the diameter of 12.7 mm and the length of 50.8 mm. The rod was placed on top of the indenter, hosted by a rubber o-ring. The assembly was inside a stainless steel frame with a transparent polycarbonate (PC) tube secured at top, which guided a 7.7 kg stainless steel cylindrical hammer. The drop distance was 16 cm. An Omega TT-K-40-25 type-K gage 40 thermal couple was attached to the cell case, about 5.0 mm away from the center (figure 1). The cell temperature was measured by an Omega OM-EL-USB-TC temperature logger.

3. Results and discussion

Cycle life measurement is conducted on cathode half-cells. Compared to the graphite anode in a full cell, the lithium anode in a half-cell is more prone to dendrite growth and limited coulombic efficiency during cycling, as it is more thermodynamically unstable in organic solvents [14]. Figure 2 shows typical cycling performance of reference cathode half-cells and CBMP-modified cathode half-cells. The discharge capacity is normalized by the capacity of the second discharge cycle. With everything else being the same, addition of 1 wt% CBMP does not cause any increase in degradation rate, since the chemical composition of CBMP is identical to CB. The major difference between CBMP and CB is the particulate size, and its effect is reduced by keeping the CBMP surfaces hydrophilic. The high degree of hydrophilicity ensures a relatively strong van der Waals bonding between the CBMP fillers and the matrix, during slurry processing as well as the cycle life testing. The electrode is processed using the wet slurry casting method and NMP is used as the solvent for the PVDF binder. Due to its high degree of hydrophilicity, CBMP attracts the NMP-PVDF solution; thus, PVDF can be effectively distributed around the CBMP and adhere to them. However, as the uniformity of PVDF distribution around active materials is affected, the overall strength and conductivity of the electrode tend to be lower.

When 2 wt% CBMP is added to the electrode, the cycle life performance of the modified half-cells is considerably reduced, which should be attribute to the volume mismatch between the CBMP fillers and the matrix. The average size of CBMP is 45–50 μm (figure 3(a)), only slightly smaller than the electrode thickness (60–70 μm) and much larger than the particle size of the active material (10–20 μm). With a relatively high volume fraction (figures 3(b) and (c), CBMP may block volumetric changes of active materials [15], and consequently, defects may be nucleated. In addition, the effect of high hydrophilicity of CBMP might have also played a

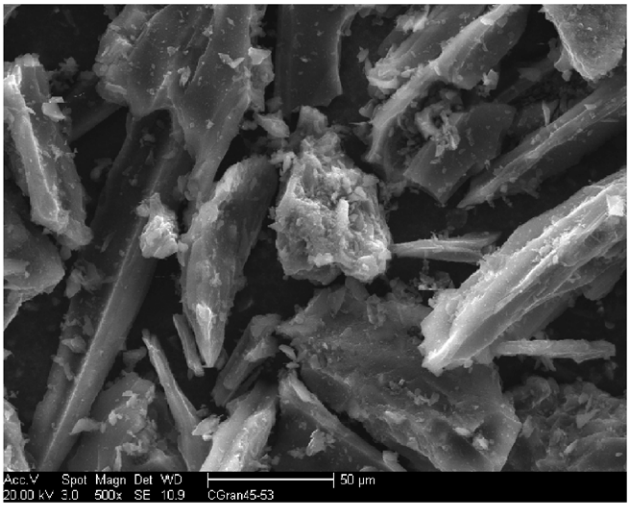

(a)

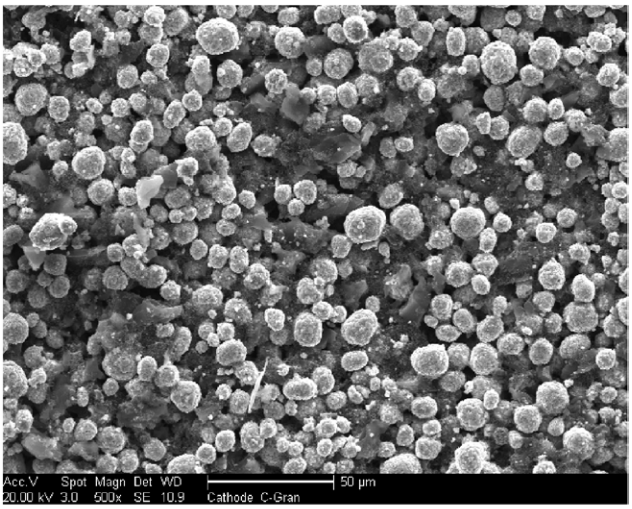

(b)

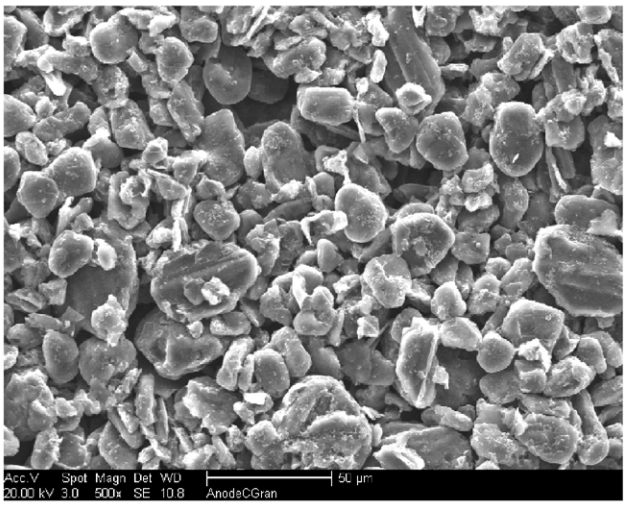

(c)

Figure 3. Typical SEM images of (a) CBMP, (b) CBMP-modified cathode, and (c) CBMP-modified anode. The CBMP content is 1 wt%.

role, by promoting the heterogeneous dispersion of PVDF. Figure 3(a) shows the raw CBMP material, and figures 3(b) and (c) show the CBMP modified cathode and anode electrodes, respectively. All images are of the same scale, with the CBMP content of 1 wt%. Even though the raw CBMP particles appear large in figure 3(a), they are not immediately detectable on the surfaces of the CBMP modified cathode and anode, suggesting that the large CBMP particles have been well embedded within the electrode matrix. During wet stage of slurry processing, the highly porous and hydrophilic CBMP particles attract the NMP-PVDF solution, interrupting the arrangement of PVDF-CB around the active materials and leading to a segregation of the PVDF-CB conductive matrix in the vicinity of the CBMP. As a result, the strength of the CBMP modified electrodes is weaker, and the conductive matrix in the CBMP modified electrodes is relatively non-uniform. The optimum CBMP cotent should be determined by the balance between the weakening effect of electrode and the increase in internal impedance. According to our data, it is around 1 wt%, discussed below.

Figure 4 shows typical temperature increase profiles in nail penetration tests. Temperature is measure 2.5 mm away from the center of the cell (figure 1), where the nail is driven through. Nail test reflects a simplified condition of internal short circuit formation, where no significant mechanical loading is involved. When a metallic nail penetrates a cell, the cathode and the anode are shorted, generating a large internal current accompanied by an extensive heat release. In a large pouch cell, the temperature increase (ΔT) often rapidly reaches more than 100 °C, which triggers thermal runaway [16]. For the coin cells in the current study, due to the large specific surface area, heat transfer would much reduce the temperature rise, and the peak temperature increase (ΔT_{max}) is only a few °C. To best simulate the thermal effects of a large ΔT, some cells are preheated.

Upon the nail penetration, in a non-preheated reference cell, the temperature increases by ~5 °C in 10–15 s. The rapid heat generation is a result of short circuit, where a sequence of rapid chemical reactions take place as the electrons quickly travel across anode and cathode charge collectors through the conductive nail [17, 18]. As heat generation continues, it competes with heat transfer [19]. Eventually, ΔT enters a plateau region for ~30 s, followed by a gradual temperature decrease. The temperature decrease rate is around 0.2 °C min^{-1}, until the cell is nearly fully discharged and the stored electrical energy is dissipated.

After preheating, the temperature profile of a reference cell is quite similar with that of a non-preheated cell, except that after the peak temperature increase, ΔT_{max}, is reached, the temperature decrease rate is reduced to 0.1 °C min^{-1} by nearly 50%. The slower temperature decrease suggests a more aggressive heat generation, probably because the electrode structure is altered and the internal impedance is lowered. It may also be related to the re-arrangement of the electrode components to a more confined configuration with better contact between active materials and CBMP, which facilitates a lasting reaction. Preheating better fits with the situation of a large pouch battery cell, where local temperature reaches more than 100 °C in thermal runaway. The lower ΔT_{max} of preheated cells should be associated with the slight voltage

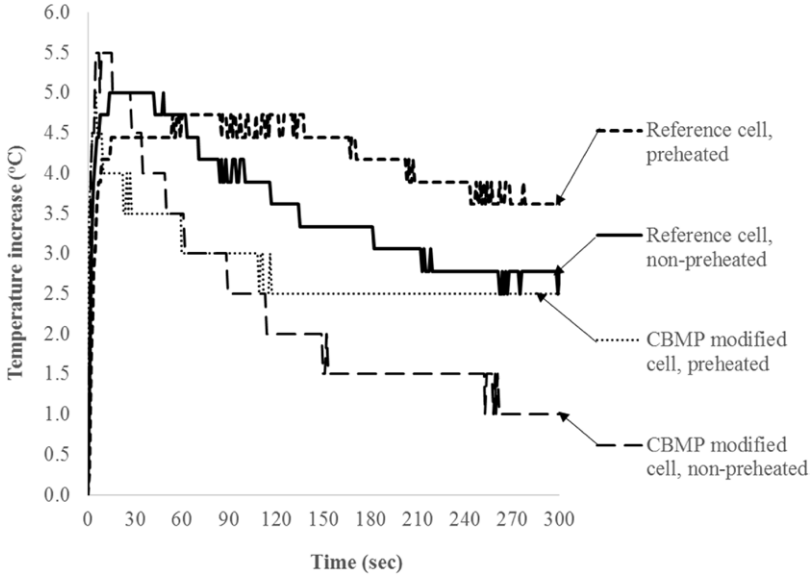

Figure 4. Typical temperature profiles in nail penetration tests.

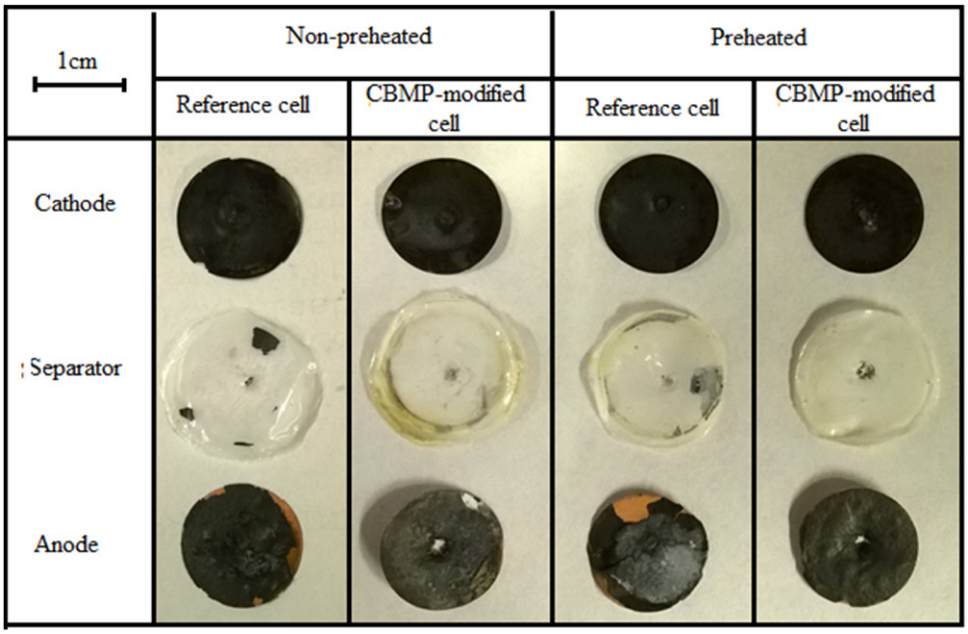

Figure 5. Photos of typical cell components after nail penetration tests.

drop after preheating, around 80–120 mV for both reference and modified cells.

As the electrode is modified by CBMP, the temperature profile changes substantially. After the peak temperature is reached, the temperature decrease rate of a non-preheated cell largely rises to about 0.4 °C min^{-1}, implying that the heat generation rate is reduced by nearly 50%. In a preheated cell, the average temperature decrease rate is around 0.2 °C min^{-1}. The reduction in heat generation rate may be caused by the impedance increase of the CBMP modified electrode. As the large CBMP particles are added in the electrode, the internal bonding among electrode components and overall conductivity are hampered. The high porosity of CBMP may be also an important factor, as CBMP can serve as electrolyte reservoirs. From figure 5, it can be seen that in both modified cathode and modified anode, the structurally altered areas with signature whitish color changes are larger than in reference electrodes. In these areas, the charge transfer is blocked and thus, the return path of internal shorting is less conductive, which lowers the heat generation rate. The effects of CBMP are more evident on anodes than on cathodes, probably due to the solid-electrolyte interface (SEI) layer formation. Debonding is observed along the interface between the modified anode layer and the copper charge collector, which also contributes to the internal impedance increase. The total generated heat, which can be assessed through the area under the temperature profile curve, is nearly the same for all the tested cells, as it should be, since the cell capacity, i.e. the amount of stored electric energy, is not affected by preheating or addition of CBMP.

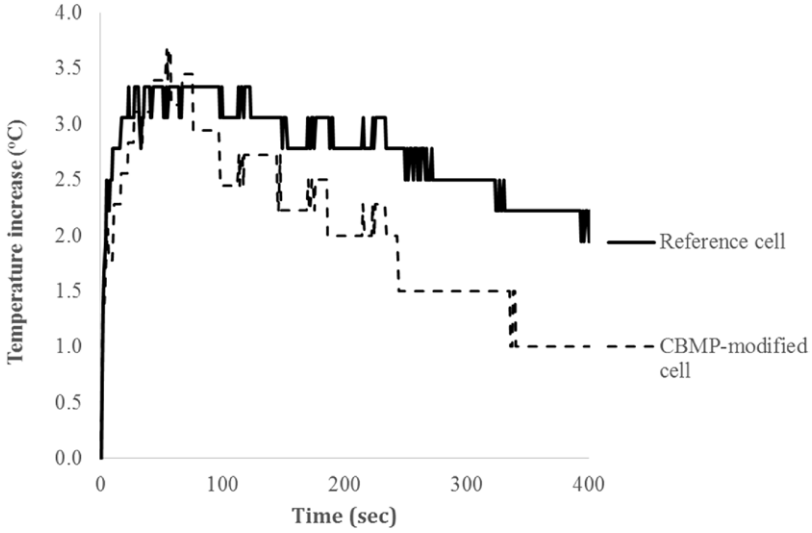

Figure 6. Typical temperature profiles in blunt impact tests.

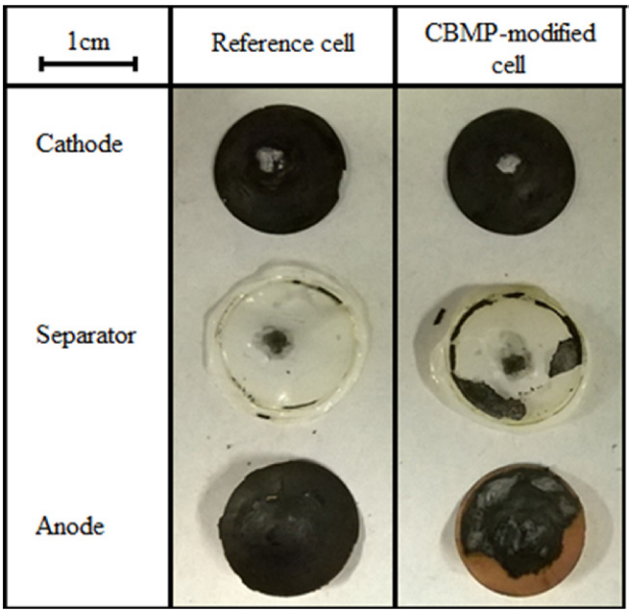

Figure 7. Photos of typical cell components after blunt impact tests.

Blunt impact tests are performed to evaluate the cell performance upon dynamic loadings. Figure 6 shows representative temperature profiles of reference and CBMP-modified battery cells. Temperature is measured 5.0 mm away from the center of the cell (figure 1), where the cell is impacted upon by a spherical brass indenter of ¼' diameter. Under the impact loading, even a fully discharged battery cell would exhibit a certain temperature increase around 1–2 °C, due to the rupture and friction of cell components as well as the sudden movement of thermocouple. This base temperature increase curve has been subtracted from the corrected curves in figure 6. As a battery cell is indented upon the mechanical impact, the indenter compresses the cathode, the membrane separator, and the anode. The membrane separator fails, so that the positive and negative electrodes directly contact each other, leading to rapid exothermic short circuit reactions. Similar with the nail penetration test, a significant temperature increase, ΔT, is detected. The temperature rises to the peak value in about half a minute. The peak temperature change, ΔT_{max}, is nearly 3.5 °C. Both of the peak temperature and the temperature increase rate are lower than that of nail experiments since the impact loading also causes physical damages in the electrodes, leading to loosened contacts among local electrode components, which slows down the exothermic reactions. The post-peak temperature decrease rate of the reference cell is nearly 0.2 °C min^{-1}, twice as much as that of nail test, which, again, suggests that heat generation is less aggressive. With the addition of 1 wt% CBMP, the temperature decrease rate increases to about 0.4 °C min^{-1}, around 2 times higher than that of the reference cell, compatible with the results of the nail penetration experiments. Clearly, the CBMP fillers weaken the electrode. As the impact happens, widespread damaging takes place and therefore, the internal impedance increases, which can be seen from figure 7. Compared with the reference cell, the CBMP modified cathode does not exhibit much difference, while the modified anode is much weakened. The weakening of the anode is desirable, because the 'bottleneck' that limits the performance of a lithium-ion battery is usually the cathode, not the anode [20].

4. Concluding remarks

To summarize, the cycling performance and mechanical abuse responses of carbon black micro-particulate (CBMP) modified lithium-ion batteries are investigated. Addition of up to 1 wt% of CBMP does not affect the cycle life; while if the CBMP content is too high, the structural integrity of the electrodes would be poor. With 1 wt% of CBMP in cathode and anode, upon nail penetration or blunt impact, the temperature increase rate and the peak temperature are similar with that of the reference cell. However, in both nail and impact tests, the temperature decrease rate of the modified cell is higher by a factor of two, suggesting that the heat generate rate is reduced. This phenomenon should be attributed to the

weakening effects of CBMP, which increases the internal impedance. Preheating at 100 °C does not have a pronounced influence on the temperature increase rate and the peak temperature, yet the post-peak temperature decrease rate is reduced.

Acknowledgment

This research is supported by the Advanced Research Projects Agency—Energy (ARPA-E) under Grant No. DE-AR0000396.

References

[1] Liu C, Li F, Ma L-P and Cheng H-M 2010 Advance materials for energy storage *Adv. Mater.* **22** E38–62
[2] Beguin F, Frackowiak E and Lu M 2013 *Supercapacitors: Materials, Systems and Applications* (NewYork: Wiley)
[3] Park J, Park M, Nam G, Lee J and Cho J 2015 Zinc-air batteries: all-solid-state cable-type flexible zinc–air battery *Adv. Mater.* **27** 1395
[4] Xu Q and Zhao T S 2015 Fundamentals for flow batteries *Prog. Energy Combust. Sci.* **49** 40–58
[5] Liang X, Garsuch A and Nazar L F 2015 Sulfur cathodes based on conductive mxene nanosheets for high-performance lithium–sulfur batteries *Angew. Chem. Int. Edn* **54** 3907–11
[6] Torreglosa J P, García P, Fernández L M and Jurado F 2014 Predictive control for the energy management of a fuel-cell–battery–supercapacitor tramway *IEEE Trans. Industr. Inform.* **10** 276–85
[7] Xiong G, Meng C, Reifenberger R G, Irazoqui P P and Fisher T S 2014 A review of graphene-based electrochemical microsupercapacitors *Electroanalysis* **26** 30–51
[8] Li J, Daniel C and Wood D 2011 Review—materials processing for lithium-ion batteries *J. Power Sources* **196** 2452–60
[9] Donnet J-B 1993 *Carbon Black: Science and Technology* 2nd edn (Boca Raton: CRC) pp 283–5
[10] Weicker P 2013 *A System Approach to Lithium-Ion Battery Management* (Norwood, MA: Artech)
[11] Balakrishnan P G, Ramesh R and Kumar T P 2006 Review—safety mechanism in lithium ion batteries *J. Power Sources* **155** 401–14
[12] McClintock F A and Argon A S 1966 *Mechanical Behaviors of Materials* (Addison-Wesley)
[13] Le A V, Wang M, Shi Y, Noelle D, Qiao Y and Lu W Effects of addition of multiwall carbon nanotubes on impact behaviors of $LiNi_{0.5}Mn_{0.3}Co_{0.2}O_2$ battery electrodes *J. Appl. Phys.* submitted
[14] Aurbach D, Zinigrad E, Cohen Y and Teller H 2002 A short review of failure mechanisms of lithium metal and lithiated graphite anodes in liquid electrolyte solutions *Solid State Ion.* **148** 405–16
[15] Zheng H, Li J, Song X, Liu G and Battaglia V S 2012 A comprehensive understanding of electrode thickness effects on the electrochemical performances of Li-ion battery cathodes *Electrochim. Acta* **71** 258–65
[16] Yoshio M, Brodd R J and Kozawa A ed *Lithium-Ion Batteries—Science and Technologies* (New York: Springer) pp 32, 61
[17] Terada N, Yanagi T, Arai S, Yoshikawa M, Ohta K, Nakajima N, Yanai A and Arai N 2001 Development of lithium batteries for energy storage and EV applications *J. Power Sources* **100** 80–92
[18] Pistoia G ed 2014 *Lithium Ion Batteries: Advances and Applications* (Oxford: Elsevier) p 419
[19] Sun Y-K, Myung S-T, Park B-C, Prakash J, Belharouak I and Amine K 2009 High energy cathode material for long life and safe lithium batteries *Nat. Mater.* **8** 320–4
[20] Choi N S, Chen Z, Freunberger S A, Ji X, Sun Y K, Amine K, Yushin G, Nazar L F, Cho J and Bruce P G 2012 Challenges facing lithium batteries and electrical double-layer capacitors *Angew. Chem. Int. Edn* **54** 9994–10024